Synthesis and biological evaluation of acridine-based histone deacetylase inhibitors as multitarget agents against Alzheimer's disease

Hui-Ju Tseng, Mei-Hsiang Lin, Young-Ji Shiao, Ying-Chen Yang, Jung-Chun Chu, Chun-Yung Chen, Yi-Ying Chen, Tony Eight Lin, Chih-Jou Su, Shiow-Lin Pan, Liang-Chieh Chen, Chen-Yu Wang, Kai-Cheng Hsu, Wei-Jan Huang

PII: S0223-5234(20)30160-4

DOI: https://doi.org/10.1016/j.ejmech.2020.112193

Reference: EJMECH 112193

To appear in: *European Journal of Medicinal Chemistry*

Received Date: 9 January 2020

Revised Date: 24 February 2020

Accepted Date: 25 February 2020

Please cite this article as: H.-J. Tseng, M.-H. Lin, Y.-J. Shiao, Y.-C. Yang, J.-C. Chu, C.-Y. Chen, Y.-Y. Chen, T.E. Lin, C.-J. Su, S.-L. Pan, L.-C. Chen, C.-Y. Wang, K.-C. Hsu, W.-J. Huang, Synthesis and biological evaluation of acridine-based histone deacetylase inhibitors as multitarget agents against Alzheimer's disease, *European Journal of Medicinal Chemistry* (2020), doi: https://doi.org/10.1016/j.ejmech.2020.112193.

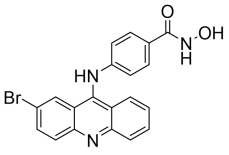

11b

Potent HDAC6 inhibitor (IC_{50} = 26 nM)
Anti-$A\beta_{1-42}$ aggregation (IC_{50} = 1.1 μM)
Strong $A\beta_{1-42}$ disaggregation (70%)
AChEI (IC_{50} = 0.88 μM)

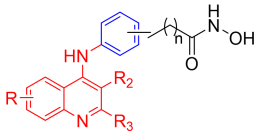

6a-d, 11a-h

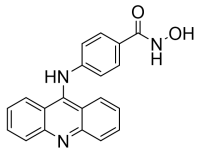

6a

Potent class IIa HDAC (IC_{50} = 0.57-2.2 μM) and HDAC6 inhibitor (IC_{50} = 25 nM)
Anti-$A\beta_{1-42}$ aggregation (IC_{50} = 3.0 μM)
$A\beta_{1-42}$ disaggregation (41%)
AChEI (IC_{50} = 0.72 μM)

Synthesis and biological evaluation of acridine-based histone deacetylase inhibitors as multitarget agents against Alzheimer's disease

Hui-Ju Tseng[a], Mei-Hsiang Lin[b], Young-Ji Shiao[c], Ying-Chen Yang[d], Jung-Chun Chu[e], Chun-Yung Chen[e], Yi-Ying Chen[f,g], Tony Eight Lin[f,g], Chih-Jou Su [f,g], Shiow-Lin Pan [f,g], Liang-Chieh Chen[f,h], Chen-Yu Wang[i], Kai-Cheng Hsu[a,f,g*], Wei-Jan Huang[a,b,e*]

[a]Ph.D. Program in Biotechnology Research and Development, Taipei Medical University, Taipei, Taiwan

[b]School of Pharmacy, Taipei Medical University, Taipei, Taiwan

[c]National Research institute of Chinese Medicine, Taipei, Taiwan

[d]Department of Biotechnology and Animal Science, National Ilan University, Ilan, Taiwan

[e]Graduate Institute of Pharmacognosy, Taipei Medical University, Taipei, Taiwan

[f] Graduate Institute of Cancer Biology and Drug Discovery, Taipei Medical University, Taipei, Taiwan

[g]Ph.D. Program for Cancer Molecular Biology and Drug Discovery, Taipei Medical University, Taipei, Taiwan

[h]School of Life and Health Sciences and Warshel Institute for Computational Biology, The Chinese University of Hong Kong (Shenzhen), Shenzhen, Guangdong, P. R. China

[i] TaiMed Biologics Inc., Taipei, Taiwan

Abstract

Multitarget agents simultaneously trigger molecules in functionally complementary pathways, and are therefore considered to have potential in effectively treating Alzheimer's disease (AD), which has a complex pathogenetic mechanism. In this study, the HDAC inhibitor core is incorporated into the acetylcholine esterase (ACE) inhibitor acridine–derived moiety. Some resulting compounds exhibited higher class IIa HDAC (4, 5, 7, and 9)- and class IIb HDAC6-inhibiting activity than did the reference SAHA as a pan-HDAC inhibitor in clinical practice. One of these compounds, **11b,** displayed greater selectivity toward HDAC6 than other isoform enzymes. In contrast, the activity of compound **6a** was selective toward class IIa HDAC and HDAC6. These two compounds exhibited strong activity against Aβ-aggregation as well as significantly disrupted Aβ-oligomer. Additionally, **11b** and **6a** strongly inhibited AChE. These experimental findings demonstrate that compounds **11b** and **6a** are multiple HDAC-Aβ-aggregation-AChE inhibitors. Notably, they can enhance neurite outgrowth, but with no significant neurotoxicity. Further biological evaluation revealed the various cellular effects of multitarget compounds **11b** and **6a**, which have the potential to treat AD.

Keywords: Histone deacetylase; Acetylcholine esterase; Acridine; Multitarget

*Corresponding authors
E-mail: wjhuang@tmu.edu.tw (W.-J. Huang)
E-mail: piki@tmu.edu.tw (K.-C. Hsu)

Introduction

Owing to the developments in healthcare, the elderly population worldwide is increasing rapidly. Aging-related diseases including cardiovascular disease, cancer, arthritis, dementia, cataract, osteoporosis, diabetes, hypertension and Alzheimer's disease (AD) have become important issues. The prevalence of Alzheimer's disease (AD) is increasing gradually. According to statistics from the American Alzheimer's association, the population with AD in 2018 was estimated to be 5.7 million. In the US in 2017, AD was the third most common cause of death of older people, behind only heart disease and cancer. Accordingly, AD has a great impact on health, welfare and economic development.

AD is characterized by progressive memory loss, a decline in language skills, and other cognitive impairments. Although its etiology is yet to be fully clarified, studies have demonstrated that AD has multiple causes, including amyloid-β (Aβ) aggregation, tau protein hyperphosphorylation, acetylcholine deficiency, genetic mutations, brain trauma, oxidative stress, neuroinflammation, and Ca^{2+}-induced neurotoxicity [1]. The complex pathogenetic mechanism of AD causes the problem that currently used single-target drugs can only alleviate the symptom of cognitive impairment, but are incapable of slowing the progression of AD. To overcome this obstacle, a multi-target strategy or combined therapy that uses at least two drugs with synergistic effects and involves the simultaneous triggering of different molecules in

the redundant pathway that is associated with AD pathogenesis can be developed. The multi-target strategy has several advantages over combined therapy, including higher patient compliance, a low risk of drug-drug interaction, the development of new chemical entities and predictive pharmacokinetics [2, 3]. From 2015 to 2017, an estimated 21% of FDA-approved new molecular entities were multi-target drugs [4]. Therefore, the use of multi-target agents is considered to be effective for treating AD [5, 6].

Histone deacetylases (HDACs) are a group of epigenetic enzymes that can regulate gene expression without changing the gene sequence. HDACs remove acetyl group from the lysine amino acid on histone, which causes the condensed nucleosome structure to inhibit gene expression. Moreover, HDAC regulates the acetylation of some nonhistone proteins such as tubulin, HSP90 and P53. These findings reveal that HDAC controls a wide range of cellular events [7, 8]. HDACs comprise 18 isoform enzymes that fall into four classes according to their sequence homology, cofactor, and intracellular distribution. Increasing evidence indicates that these HDAC enzymes are associated with learning, memory formation and neuroplasticity. Further, dysregulation of histone acetylation and deacetylation is observed in AD mice models and AD patients [9, 10]. For example, in the transgenic mice model, the overexpression of HDAC2 reduces dendritic spine density, synaptic number and

synaptic plasticity, and impairs memory formation[11]. One investigation has revealed that HDAC4 overexpression induces neurotoxicity, which is related to neurodegeneration [12]. HDAC6 levels are substantially increased in the hippocampus and cortex of the AD patient brain and this enzyme is implicated in tau hyperphosphorylation [13]. Hyperphosphorylated tau protein has been demonstrated to induce the formation of intracellular neurofibrillary tangles (NFTs), which cause synaptic dysfunction and neuron impairment [14]. The inhibition of HDAC6 suppresses the phosphorylation of tau, stabilizing the HDAC6-tau complex [15]. Furthermore, HDAC6 inhibition downregulates Aβ aggregation [16] and alleviates cognitive impairment in an *in-vivo* AD mouse model [13]. Importantly, several HDAC inhibitors, such as 4-phenylbutrate, valproic acid, vorinstat (SAHA) [17] and MS 275 [18], exhibit *in-vitro* and *in-vivo* activity and thus improve cognition. These findings indicate that HDAC has a crucial role in AD and HDAC enzymes may be targeted to treat AD.

Only four drugs - rivastigmine, galantamine, donepezil, and memantine - have been developed to treat AD [1]. The first three are acetylcholine esterase (AChE) inhibitors, which can prevent the degradation of acetylcholine into choline and acetic acid and thus increase acetylcholine levels in the synapse of CNS, alleviating cognition deficits that are associated with AD. The last one, memantine, an NMDA

receptor antagonist, attenuates Ca^{2+}-induced neurotoxicity. These four compounds have limited therapeutic outcomes as they alleviate some symptoms but cannot slow the progression of AD [1]. This result is explained by the fact that AD is caused by multiple molecular abnormalities rather than a single defect. Simultaneously triggering molecules in functionally complementary pathways may provide synergistic effects.

Numerous structurally diverse multifunctional agents that act on different biological targets relevant to AD etiology have been discovered in attempts to solve the clinical problems of current anti-AD drugs (Fig. 1). Some compounds have advanced to clinical trials. For example, a tacrine-indole hybrid NP-61 has been identified as a dual inhibitor of AChE and Aβ secretion, but was withdrawn in phase 1 of a clinical study [19]. Compound **1,** derived from donepezil, exhibits AChE and selective monoamine oxidase A (MAO) inhibition and functions as an antioxidant and Cu^{2+} chelator [20]. Similarly, ladostigil, which contains rivastigmine that is fused with a rasagiline motif, exhibits enzyme inhibition against AChE and MAO and antioxidative activity [21]. Compound **2**, which comprises tacrine in combination with a nimodipine motif, inhibits AChE as well as Aβ aggregation and secretion, and blocks the Ca^{2+} channel [22]. Ladostigil and BGC20-1259 have advanced to a clinical study. These results demonstrate that multifunctional agents may have the potential

effectively to target the etiologically complex AD.

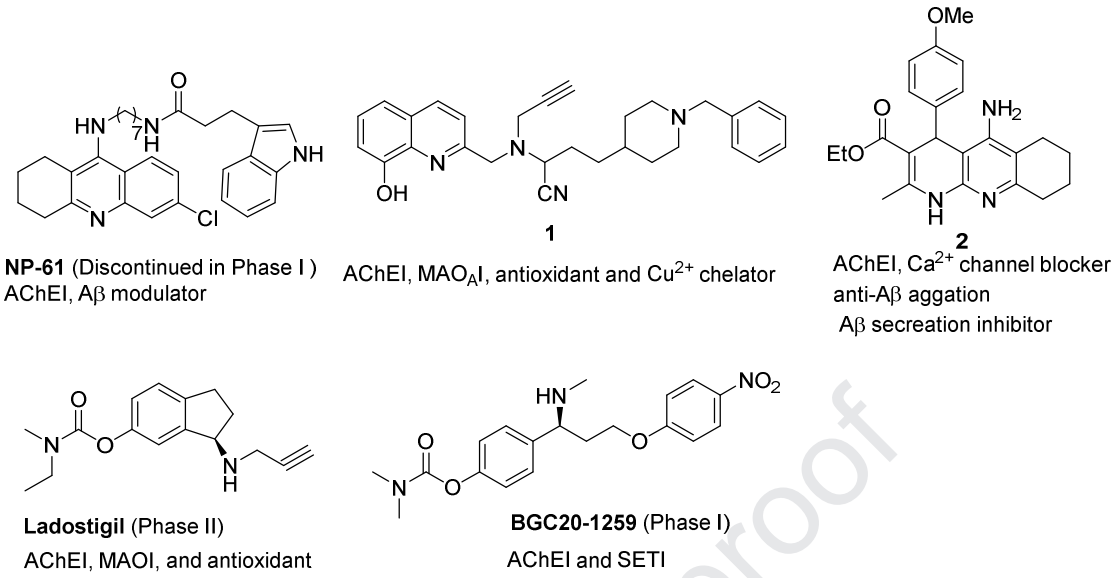

Figure 1. Identified multitarget-directed ligands against AD.

Acridine, which is a structurally diverse scaffold, is commonly used for anti-AD drug design[23]. For example, 9-aminotetrahydroacridine (tacrine) exhibited potent AChE inhibitory activity (Fig. 1S). Compound **12** that contains acridine-tetrahydroacridine hybrid is demonstrated to show much higher activity than tacrine (Fig. 1S), which suggests that acridine group contributed to anti-AChE effect[24]. Acridine derivative **25** exhibited potent inhibitory activity against Aβ aggregation [25] (Fig. 1S). Additionally, it displayed high blood-brain barrier (BBB) permeability. The structure-activity relationship (SAR) study reveals that the planar structure of acridine greatly contributed to Aβ aggregation-inhibiting activity[26]. Recently, Jiang and coworkers used a hybrid of acridine derivative and pyridothiaoxazole scaffold of a glycogen synthase kinase-3β (GSK-3β) inhibitor to

develop a series of multitarget inhibitors [27]. One of these compounds, **2f,** not only exhibited potent enzyme-inhibiting activity against GSK-3β and AChE, but also inhibited Aβ aggregation (Scheme 1), which indicates chemical conjugation at the C-9 position of acridine moiety can generate novel multitarget agents without significantly reducing its anti-AChE effect. These findings suggest acridine derivatives can be considered as an effective ligand for the design of multitarget-directed agents against AChE and Aβ associated with AD pathology owing to its simple structure and high ligand efficiency [28, 29]. Givinostat is a HDAC inhibitor currently under clinical study[30]. It contains a phenylhydroxamic acid moiety as a core scaffold for enzyme-inhibiting activity. In addition to givinostat, this scaffold is also found in various HDAC inhibitors such as PCI-24781[31], tubastatin A [32], and NCC149 [33](Fig 2S).

Based on the roles of HDAC, Aβ protein and AChE inhibitors in AD as mentioned above, the simultaneous targeting of AChE, HDAC and Aβ may have a synergistic anti-AD effect. We sought to develop a multiple target agent possibly as an effective strategy against AD. In the present work, we incorporated phenylhydroxamic acid core of givinostat into C-9 position of various acridine–derived moieties using nitrogen as a connecting unit (Scheme 1). Novel series of acridine derivative-bearing phenylhydroxamic acids were synthesized. The SAR of the resulting compounds that

inhibited various HDAC isoforms was disclosed. Of these compounds, **11b** exhibited more selectivity toward HDAC6 than other isoform enzymes (Scheme 1). In contrast, compound **6a** showed selective inhibition against class IIa HDAC and HDAC6 (Scheme 1). These acridine derivative-containing compounds were further evaluated for inhibitory activities against Aβ aggregation as well as AChE. We found that both compounds **11b** and **6a** not only exhibited strong activity against Aβ-aggregation, but also showed strong AChE inhibition. These experimental findings identified compounds **11b** and **6a** as multitarget inhibitors of HDAC, Aβ-aggregation, and AChE. The analysis of molecular docking revealed the structural difference between these two compounds when bound to class IIa and class IIb HDAC. Furthermore, they can promote neurite outgrowth in mice hippocampus cells without significant neurotoxicity. Further experiments on microsome stability and blood-brain barrier (BBB) permeability were performed and revealed the potential of the resulting compounds against AD.

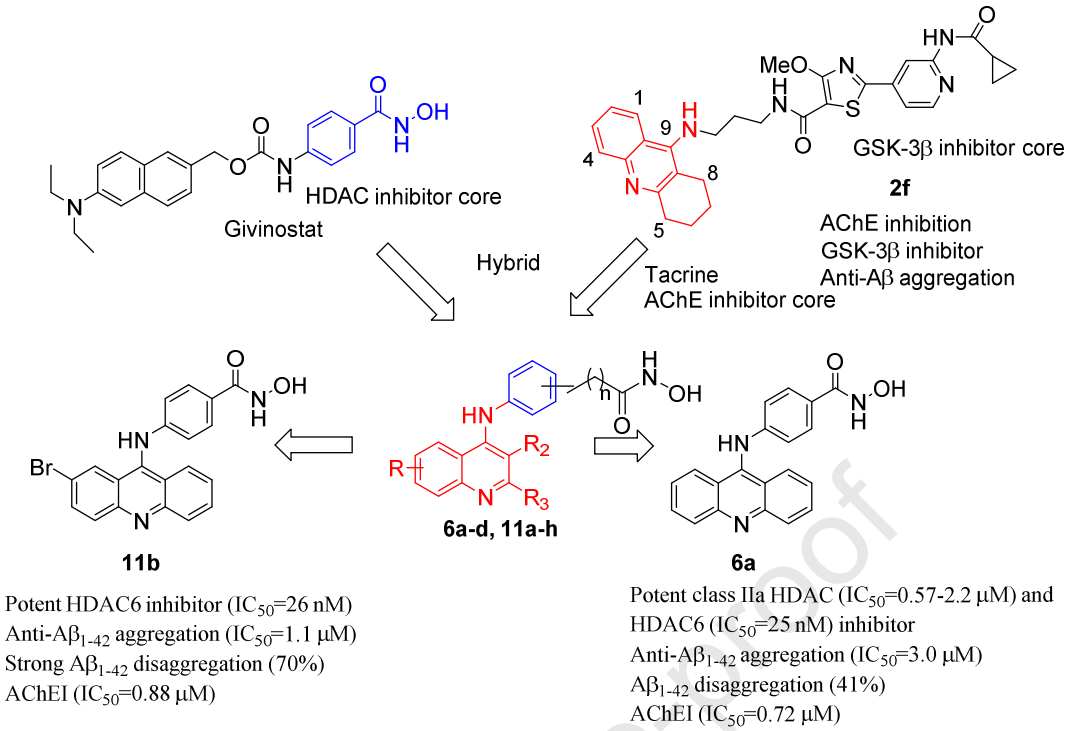

Scheme 1. Compounds **6a** and **11b** using a hybrid of givinostat and compound **2f** as multitarget inhibitors of HDAC, Aβ and AChE

1. Chemistry

The hydroxamates **5a-d** were synthesized as described in Scheme 2. Methyl esters **3a-c** with different carbon linker chain-lengths reacted with NH_2OH under basic conditions to give hydroxamates **4a-c**, respectively. Compounds **4a-c** coupled with 9-chloroacridine **5** using 2-methoxyethanol yielded corresponding compounds **6a-c**. Using the described synthetic methodology, compound **6d** was synthesized staring from **3d**.

Scheme 2

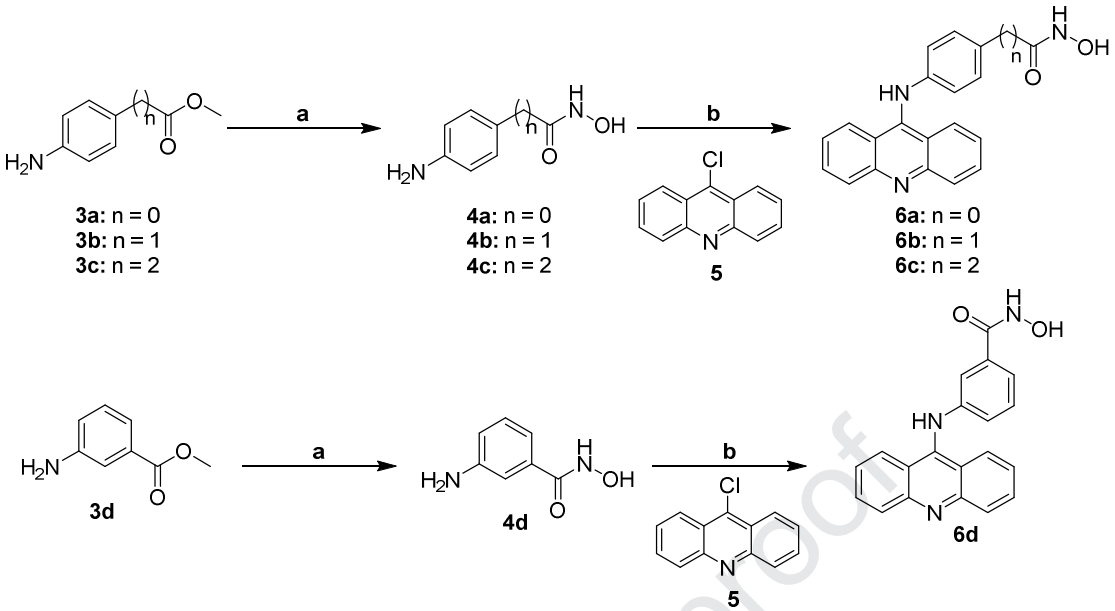

Reagents and conditions: (**a**) **i**) THF/MeOH, 0 ^{o}C; **ii**) 50%$NH_2OH_{(aq)}$, NaOH, RT; (**b**) $CH_3O(CH_2)_2OH$, 12N HCl, 0 ^{o}C-RT.

Compounds **11a-h** were synthesized as described in Scheme 3. Ullmann coupling of 2-iodobenzoic acid **7** with different substituted aniline **8a-e** provided **9a-e**, respectively. Friedel-Crafts acylation followed by the chlorination of **9a-e** yielded corresponding 9-chloroacridines **10a-e**. Compounds **10a-h** coupled with compound **4a** in the presence of 2-methoxyethanol afforded **11a-h**, respectively. Details on the synthesis, isolation and characterization of compounds **4** and **9-10** can be found in the supplementary material. The estimated purity of compounds **6a-6d** and **11a-11h** is at least 97% as determined by HPLC analysis (supplementary material).

Scheme 3

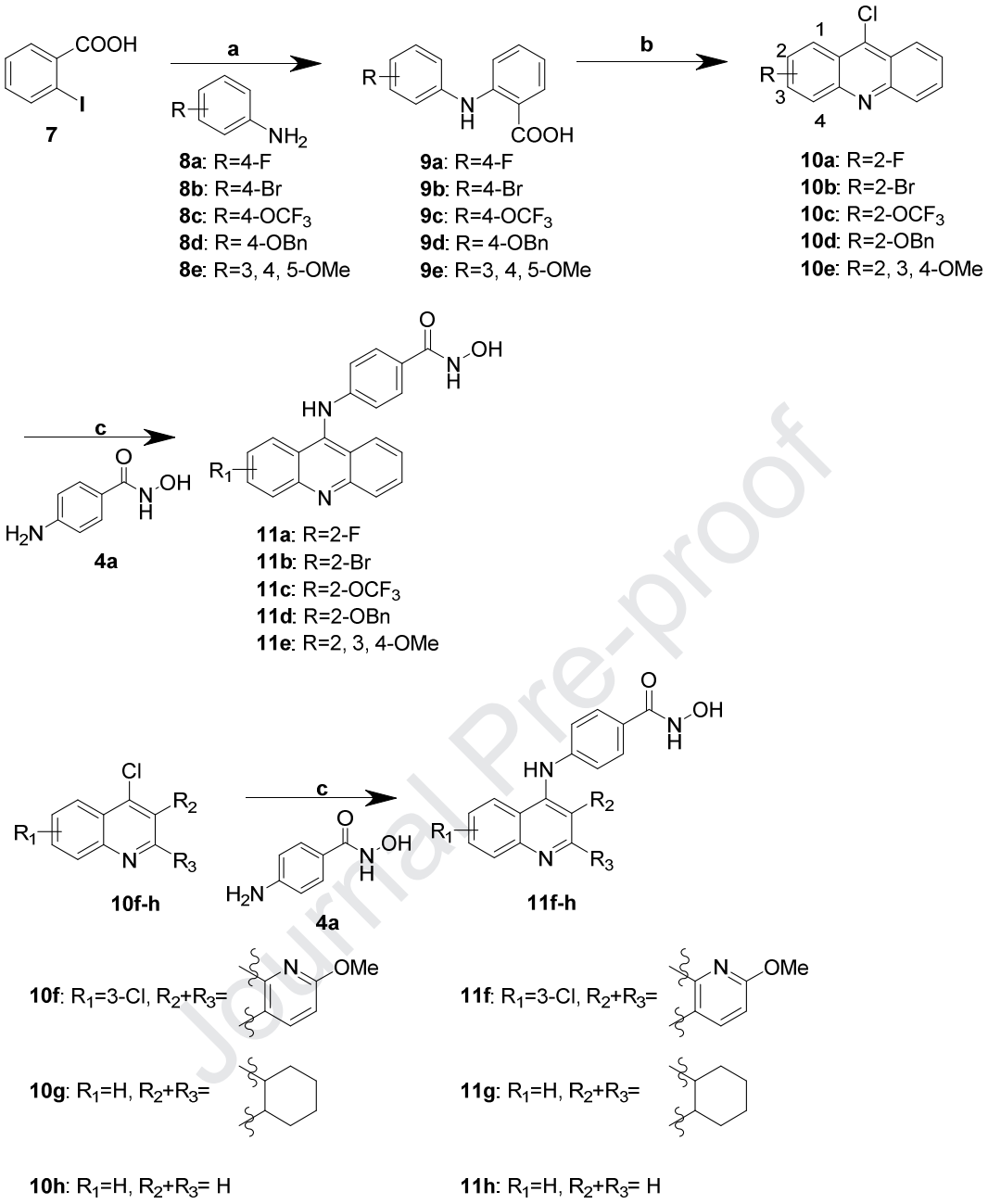

Reagents and conditions: (**a**) K_2CO_3, CuI, Cu, DMF, 150 ^oC; (**b**) $POCl_3$, 130 ^oC; (**c**) $CH_3O(CH_2)_2OH$, 12N HCl, 0 ^oC-RT.

2. Results and discussion

3.1 HDAC-inhibiting activity

Compounds **6a-d** were tested to determine their enzyme inhibitory activity

against a panel of HDAC isoforms, including HeLa nuclear HDACs, class IIa HDAC (4, 5, 7, 9) and class IIb HDAC (6), using SAHA as a reference (Table 1). Most HeLa nuclear HDACs contained class I HDACs. Of the four compounds, compound **6a** exhibited more potent activity than SAHA against class IIa and class IIb HDACs. Of the compounds **6a-c** with different carbon chain linker between aminoacridine and hydroxamic acid, compound **6a** was the most potent, suggesting that the phenyl linker contributed greatly to enzyme inhibitory activity. In contrast, compound **6d** exhibited low activity, suggesting *meta*-substituted acridine negatively contributed to activity. These experimental results motivate the synthesis of compounds **11a-h** bearing varied acridines at the *para*-position of phenylhydroxamate.

Table 1

IC_{50}[a] value (μM) of compounds **6a-d** for HDACs inhibition

Compound	Class I	Class IIa				Class IIb
	HeLa nuclear HDAC	HDAC4	HDAC5	HDAC7	HDAC9	HDAC6
6a	0.55 ± 0.03	2.24 ± 0.06	0.85 ± 0.07	0.65 ± 0.03	0.57 ± 0.02	0.025 ± 0.00
6b	2.07 ± 0.26	26.63 ± 5.38	1.66 ± 0.30	1.94 ± 0.03	6.42 ± 0.39	0.074 ± 0.00
6c	0.10 ± 0.03	7.06 ± 1.10	2.58 ± 0.47	31.53 ± 2.98	28.96 ± 0.89	0.14 ± 0.00
6d	> 40	29.38 ± 0.96	20.76 ± 3.93	16.84 ± 0.50	12.18 ± 1.15	4.69 ± 0.19
SAHA	0.034 ± 0.00	33.04 ± 6.85	10.51 ± 0.86	> 40	32.26 ± 1.60	0.083 ± 0.00

[a]Data are obtained from three independent experiments.

The experimental results reveal that compounds **11a-c** exhibited higher class IIa and class IIb HDAC inhibiting activity than SAHA (Table 2). Compound **11a** exhibited greater activity against class I HDACs and retained the activity toward other isoforms, compared to compound **6a**. This experimental result indicates that the C-2 fluoro substituent of acridine broadened the spectrum of anti-HDAC activity. However, compounds **11b** and **11c** with C-2-bromo and -OCF_3, respectively, exhibited weaker activity than compound **11a** against class IIa HDACs. Compound **11d** with the C-2 OBn group displayed selectivity toward HDAC4 and 5 over other isoform enzymes. Compound **11e** with the C-2, -3 and -4 methoxy groups had lower activity against most HDAC enzymes. Similarly, compound **11f** with C-2 chloro and C-7 OMe exhibited weaker activity. Compound **11g** with the tacrine moiety showed much weaker activity toward all enzymes than compound **6a**, suggesting that the coplanar tricyclic skeleton greatly contributed to activity. Interestingly, compound **11h** with quinolone exhibited HDAC6-selective inhibition.

Table 2

IC_{50}[a] value (μM) of compounds **11a-h** for HDACs inhibition

Compound	Class I	Class IIa				Class IIb
	HeLa nuclear HDAC	HDAC4	HDAC5	HDAC7	HDAC9	HDAC6
6a	0.55 ± 0.03	2.24 ± 0.06	0.85 ± 0.07	0.65 ± 0.03	0.57 ± 0.02	0.025 ± 0.00
11a	0.25 ± 0.01	3.04 ± 0.73	0.69 ± 0.04	0.59 ± 0.06	0.52 ± 0.03	0.029 ± 0.00
11b	0.16 ± 0.00	7.85 ± 0.68	7.19 ± 0.47	9.13 ± 0.30	5.51 ± 0.07	0.026 ± 0.00
11c	0.67 ± 0.19	14.71 ± 4.31	15.83 ± 1.92	17.88 ± 1.54	31.10 ± 1.45	0.029 ± 0.00
11d	3.50 ± 0.41	1.21 ± 0.06	0.43 ± 0.09	3.10 ± 0.30	1.25 ± 0.07	0.22 ± 0.04
11e	0.81 ± 0.14	15.73 ± 0.08	4.23 ± 0.03	4.57 ± 0.04	4.95 ± 0.21	0.16 ± 0.02
11f	0.80 ± 0.06	> 40	15.18 ± 2.91	10.29 ± 0.69	> 40	0.34 ± 0.00
11g	> 40	> 40	17.54 ± 0.57	> 40	> 40	3.55 ± 0.35
11h	0.60 ± 0.00	> 40	3.37 ±0.50	32.67 ± 7.08	13.23 ± 1.29	0.039 ± 0.00
SAHA	0.034 ± 0.00	33.04 ± 6.85	10.51 ± 0.86	> 40	32.26 ± 1.60	0.083 ± 0.00

[a]Data are obtained from three independent experiments.

3.2 Inhibition of $A\beta_{1-42}$ self-aggregation

Compounds **6a** and **11a-h** were evaluated for the inhibition against $A\beta_{1-42}$ oligomerization using the Thioflavin T (ThT) assay. Morin was used as the reference compound. Compounds **6a** and **11b-d** were more potent than Morin in inhibiting $A\beta_{1-42}$ self-aggregation, as they had IC_{50} values around 3μM (Table 3). Furthermore, compounds **11b-d** and **11f** disaggregate $A\beta_{1-42}$ oligomer by more than 50% in 10 μM. In particular, compound **11b** significantly inhibited $A\beta_{1-42}$ aggregation and $A\beta_{1-42}$

oligomer disaggregation.

Table 3

Inhibitory activities [a] of compounds **6a**, and **11a-h** against $A\beta_{1-42}$ oligomerization

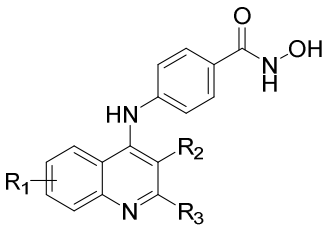

Compound	R1	R2+R3	Inhibition of $A\beta_{1-42}$[a] Aggregation IC_{50} (μM)	$A\beta_{1-42}$[a] of Disaggregation (%)
6a	H		3.0 ± 0.7	41
11a	2-F		> 20	38
11b	2-Br		1.1 ± 0.5	70
11c	2-OCF_3		3.5 ± 0.9	53
11d	2-OBn		3.0 ± 0.6	57
11e	2,3,4-OMe		13.0 ± 0.2	42
11f	3-Cl	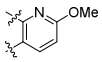	34.9 ± 6.5	53
11g	H		> 20	0
11h	H	H	> 20	0
Morin[c]			8.5 ± 0.6	ND[b]
SAHA			> 20	0

[a]Data are obtained from three independent experiments.

[b]ND: not determined.

3.3 AChE inhibiting activity

Compounds **6a** and **11a-h** were tested to evaluate their AChE-inhibiting activity (Table 4). Four compounds **6a**, **11a-b**, **11e**, and **11h** exhibited comparable activities with IC_{50} values in the range of 0.6-0.8 μM.

Table 4

IC_{50}[a] value (μM) of AChE inhibitory activity of compounds **6a**, and **11a-h**

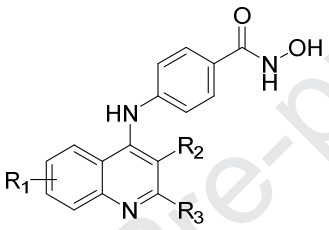

Compound	R1	R2+R3	AChE
6a	H		0.72 ± 0.02
11a	2-F		0.60 ± 0.03
11b	2-Br		0.88 ± 0.05
11c	2-OCF_3		3.65 ± 0.08
11d	2-OBn		2.64 ± 0.13
11e	2,3,4-OMe		0.64 ± 0.01
11f	3-Cl	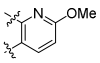	9.25 ± 0.09
11g	H		1.97 ± 0.07
11h	H	H	0.83 ± 0.01
Acridine			6.84 ± 0.06

[a] Data are obtained from three independent experiments.

3.4 Class I HDACs isoform-inhibiting activity

To confirm that compounds **6a** and **11b** were less potent than SAHA in inhibiting class I HDAC, their class I HDAC1, 2 and 3 enzyme-inhibiting activities were evaluated. The experimental results indicated that compound **6a** exhibited much lower activity against HDAC1, 2, and 3 than did SAHA. Compound **11b** exhibited less potent activity against other enzymes, except for HDAC1.

Table 5

IC_{50}[a] value (μM) of compounds **6a**, and **11b** against class I HDACs 1, 2, and 3

Compound	Class I		
	HDAC1	HDAC2	HDAC3
6a	0.34 ± 0.01	1.57 ± 0.04	1.22 ± 0.00
11b	0.09 ± 0.01	0.48 ± 0.08	0.33 ± 0.00
SAHA	0.025 ± 0.00	0.091 ±0.00	0.032 ± 0.00

[a]Data are obtained from three independent experiment.

3.5 Analysis of molecular docking of compounds 6a and 11b

To better understand the inhibition of the HDAC isozymes by the synthesized compounds, a molecular docking analysis was performed. We validated the docking protocol by docking the co-crystal ligands into their respective HDAC active sites (Fig. 3S). The docking poses of the compounds show similar conformations to their

co-crystal confirmations. This suggests a reliable docking protocol was used.

Next we selected compounds **6a** and **11b** for analysis because both showed inhibitory activity towards class IIa and IIb HDACs (Table 2). For our analysis, we selected the docking pose that not only produced the best docking score, but also coordinated to the zinc ion using its ZBG. The selected pose showed comparable docking scores to multiple solutions, which suggests a favorable docking conformation. The compounds can also be separated into three groups with respect to traditional HDAC inhibitors – ZBG, linker and cap group. Compounds **6a** and **11b** both contain a hydroxamic acid moiety that functions as the ZBG (Fig. 2). This moiety also forms hydrogen bonds with residues H611 and G619. The linker consists of an aniline moiety which spans a hydrophobic tunnel and its aromatic ring facilitates hydrophobic interactions with residues such as F620 and F680. The nitrogen on the linker forms an additional hydrogen bond with residue S568 near the periphery of the active site. The caps of both compounds are composed of different structures. Compound **6a** contains an acridine cap, whereas compound **11b** has a 2-bromoacridine cap. Both compounds have hydrophobic contacts with residue L749. Their similar inhibitory activities are attributable to their similar interactions.

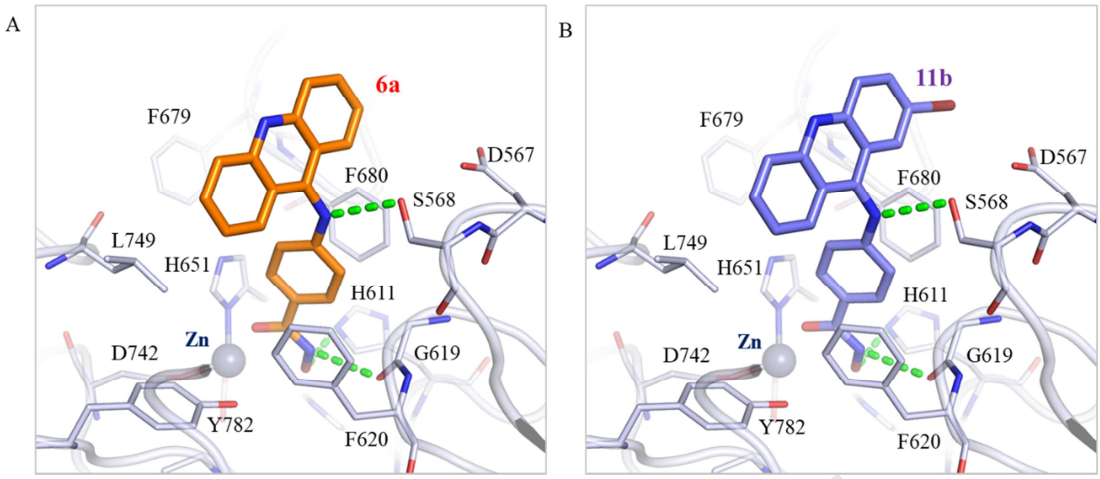

Figure 2. Docking poses of compounds **6a** and **11b** in HDAC6. The docking poses of compound **6a** (A, orange) and compound **11b** (B, purple) in the HDAC6 active site. Hydrogen bonds are represented as green dash lines. HDAC6 (grey) is represented as a stick model. Residues are labeled.

Compound **6a** inhibits class IIa isozymes. The ZBG and the linker cause HDAC7 to adopt a pose similar to that of HDAC6 (Fig. 3A). For example, the hydroxamic acid not only coordinates the zinc ion, but also forms hydrogen bonds with residues H669 and H670. The linker also hydrophobically interacts with residues F679 and H709. The acridine cap of compound **6a** hydrophobically interacts with residues F737 and F738. Both residues occupy the rim of the HDAC7 active site, which is a pocket that is favorable for the aromatic rings (Fig. 3B). The protein loops of HDAC6 and HDAC7 occupy different positions. Furthermore, HDAC6 contains residue S568 while HDAC7 contains residue D626. The orientation of the loop in HDAC6 facilitates the formation of a hydrogen bond with the linker of compound **6a**.

HDAC7 does not exhibit this interaction. The loss of a hydrogen bond interaction reduces the effectiveness of inhibiting activity of compound **6a** towards HDAC7.

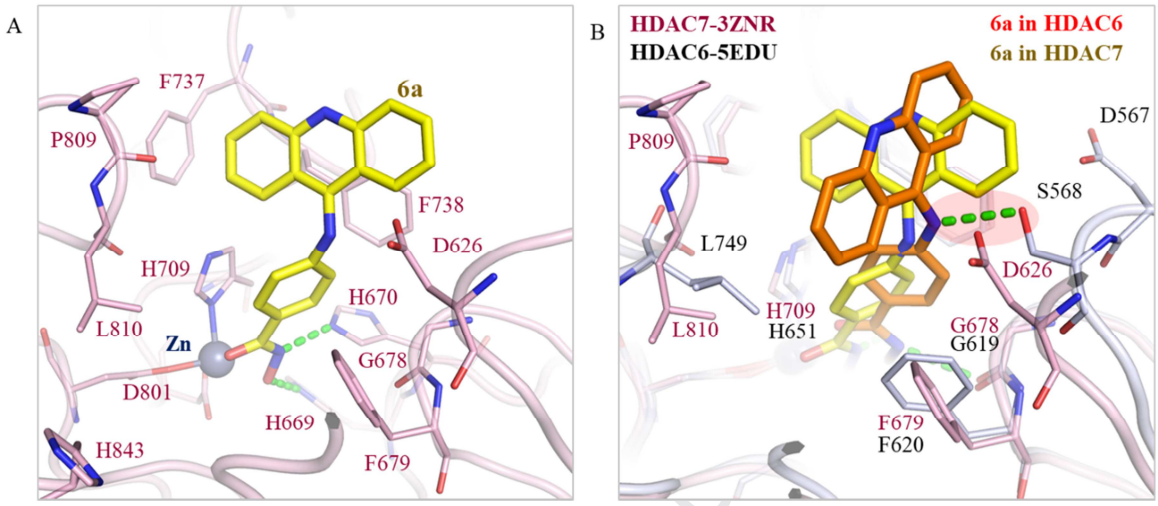

Figure 3. Comparison of docking poses of compounds **6a** in HDAC6 and HDAC7 (A) Docking pose of compound **6a** (yellow) in the HDAC7 (pink) active site. (B) Superimposed docking poses of compound **6a** in HDAC6 (orange) and HDAC7. Hydrogen bonds are denoted as green dashed lines. HDAC6 (grey) and HDAC7 (pink) are represented as stick models. Residues are labeled.

Compound **11b** exhibits even weaker inhibitory activity toward class IIa isozymes (Table 2). Compound **11b** adopts a pose similar to that of compound **6a** in HDAC7; it forms hydrogen bonds with residues H669 and H670 and hydrophobically interacts with residues F679 and F709 (Fig. 4A). However, the bromo moiety of the compound **11b** cap group sterically clashes with residues H709 and P809 (Fig. 4). In contrast, the acridine cap of compound **6a** does not extend into this pocket (Fig. 4B). This fact may explain why compound **6a** may exhibit stronger inhibiting activity than

compound **11b** toward HDAC7. Together, the cap groups of this class of compounds alter the inhibitory activities between HDAC isozymes.

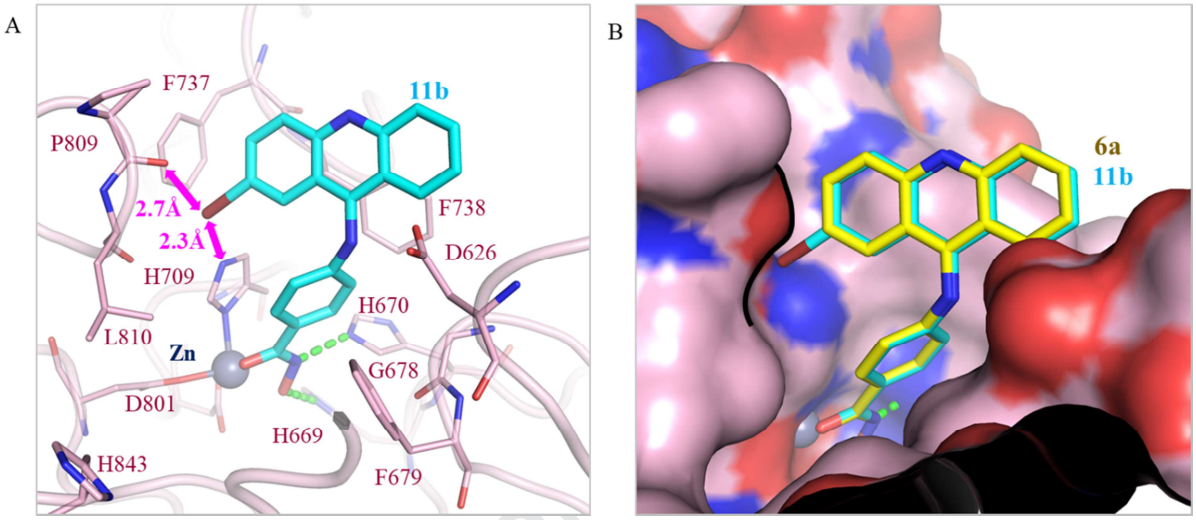

Figure 4. The cap group affects HDAC inhibitory activity. (A)Docking pose of compound **11b** (blue) in the HDAC7 (pink) active site. The distance between the bromo moiety and surface residues H709 and P809 is shown. (B) Docking pose of compound **6a** (yellow) in HDAC7 is superimposed onto pose of compound **11b** in HDAC7 (surface model). Hydrogen bonds are represented as green dashed lines. Residues are labeled.

3.6 Promotion by compounds 6a and 11b of histone H3 and α-tubulin acetylation

Histone H3 and α-tubulin are substrates of class I HDACs and HDAC6, respectively. Compounds **6a** and **11b** were incubated with murine neuroblastoma Neuro-2a cells at different concentrations using trichostatin A (TSA) as a reference compound. Western blotting revealed that compounds **6a** and **11b** dose-dependently increased the levels of acetylated histone H3 (Fig. 5). The EC_{50} values of compounds **6a** and **11b** were 7.96 and 0.58 μM, respectively. These two compounds also induced α-tubulin acetylation in a dose-dependent manner. Their EC_{50} was around 8 μM. Experimental data on the promotion of histone and tubulin acetylation were consistent with the fact that compound **11b** exhibited higher activity than did compound **6a** in inhibiting HDACs 1, 2, and 3.

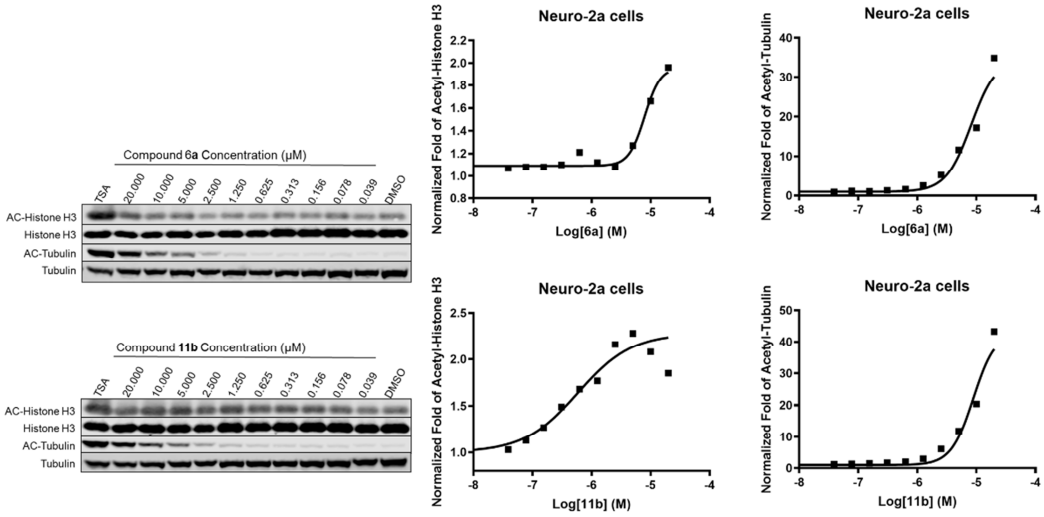

Figure 5. Induction by compounds **6a** and **11b** of histone H3 and tubulin acetylation

in mice neuroblastoma Neuro-2a cells. Western blot analysis of histone H3 and tubulin acetylation after treatment with compound **6a** and **11b** were exhibited. Neuro-2a cells were treated with various concentration of compounds **6a** and **11b** for 24 h. Protein levels after treated with compounds **6a** and **11b** were detected by Western blot analysis. Quantification analysis of Western blot was conducted using LI-COR Odyssey Fc Imaging System. The EC_{50} values of compounds **6a** and **11b** were calculated using the GraphPad Prism 4 program based on a sigmoidal dose-response equation of 10 dose concentrations using 2-fold dilution (n = 3).

3.7 Effects of 6a and 11b on cell viability in murine neuroblastoma Neuro-2a cells

Figure 6 shows the cell viabilities of murine neuroblastoma Neuro-2a cells that were incubated with compounds **6a** and **11b**. The figure indicates that both compounds, even at concentrations as high as 10 μM, only slightly affected cell viability, suggesting that both compounds exhibited low cytotoxicity.

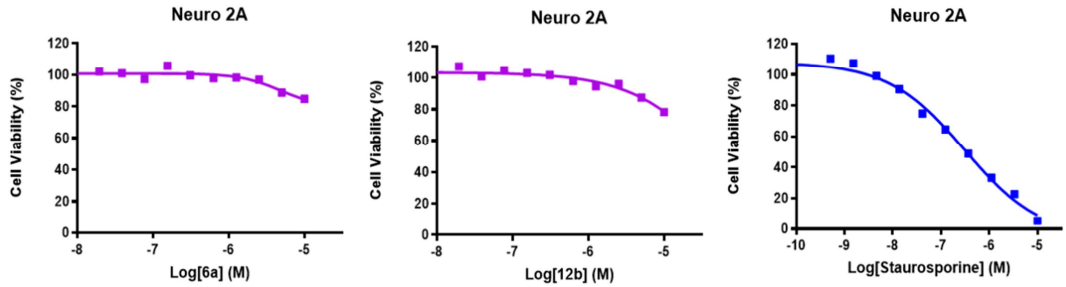

Figure 6. Effects of compounds **6a** and **11b** on cell viability of mice neuroblastoma Neuro-2a cells. The Cell Titer-Glo 2.0 Luminescent cell viability assay was used for

Neuro-2a cells that were treated with various concentration of compounds **6a**, **11b** and reference staurosporine for 24 h. The data reported are means from two independent experiments performed in triplicate.

3.8 Induction by compounds 6a and 11b of neurite outgrowth in mice hippocampus cells

To investigate the enhancement of neurite outgrowth by compounds **6a** and **11b**, primary rat hippocampus neurons were incubated with these two compounds at various concentrations of these two compounds for three days. Neuronal differentiation was identified by immunostaining. The lengths and numbers of primary, secondary, and tertiary neurites were obtained (supplementary material). Figure 7 shows that compounds **6a** and **11b** increased the number of axonal and dendritic neurites in a dose-dependent manner compared to those of control. Meanwhile, compound **11b** increased the length of axonal neurites in a dose-dependent manner (Fig. 4S). These results suggest that compounds **6a** and **11b** promote neurite outgrowth.

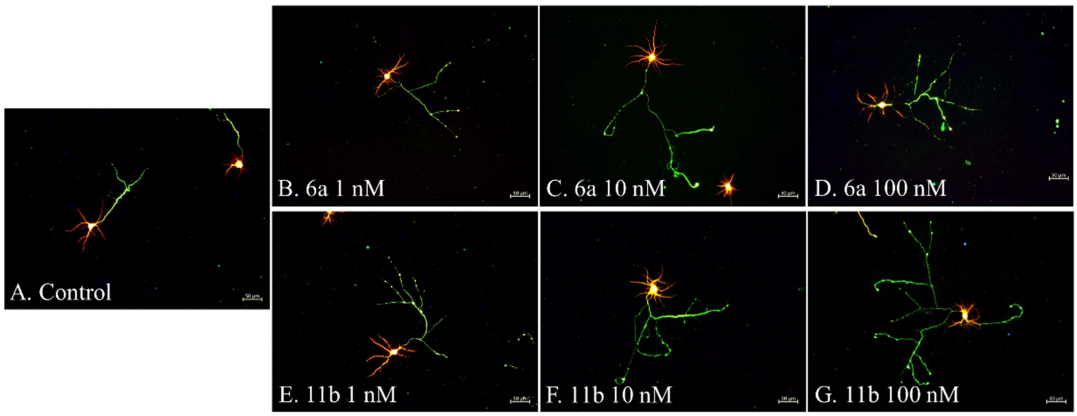

Figure 7. Promotion of hippocampal neurite formation by compounds **6a** and **11b** revealed by immunostaining with anti-tau antibody for axon recognition, anti-MAP2 antibody for dendrite recognition, and DAPI for nuclear recognition. The primary hippocampus neuron was incubated with different concentrations of compounds **6a** and **11b**.

3.9 Metabolic stability of compounds 6a and 11b against human liver microsome

The pharmacokinetic profiling of compounds **6a** and **11b** was evaluated in terms of metabolic stability against human liver microsome. The experimental results revealed that compounds **6a** and **11b** exhibited higher $T_{1/2}$ than the reference testosterone (Table 6). Both compounds had lower CL_{int}, falling into the medium class of CL_{int} classification band[34].

Table 6

Metabolic stability of compounds **6a**, **11b**, and reference compound in human liver microsomes

Compound	k (min^{-1})	$T_{1/2}$ (min)[a]	CL_{int}[b]

			(mL/min/mg protein)
6a	0.0204 ± 0.0011	33.92 ± 1.93	0.0407 ± 0.0023
11b	0.0183 ± 0.0011	37.86 ± 2.20	0.0366 ± 0.0022
Testosterone	0.0270 ± 0.0039	25.67 ± 3.51	0.0540 ± 0.0077

[a]$T_{1/2}$, $p < 0.05$ vs. testosterone. Statistical analysis was performed using one-way ANOVA followed by Bonferroni t-test.

[b]Intrinsic clearance (CL_{int}) was calculated based on $CL_{int} = k/P$, where k is the elimination rate constant and P is the protein concentration in the incubation.

3.10 Blood-brain barrier permeability of compounds 6a and 11b

Compounds **6a** and **11b** were assayed in MDR1-MDCK test to assess their BBB permeability [35-37]. Experimental data indicated that compound **11b** had moderate BBB permeability with a mean P_{app} value of 4.57 × 10^{-6} cm/s and an efflux ratio of 7.42 (Table 7). However, compound **6a** had a low BBB permeability with mean P_{app} value of 2.72 × 10^{-6} cm/s.

Table 7

MDR1-MDCK permeability of compounds **6a**, and **11b**[a]

Compound	Mean P_{app} (10^{-6} cm/s)	Efflux ratio[b]	BBB category[c]
6a	2.72 ± 0.04	17.54 ± 1.22	Low
11b	4.57 ± 0.47	7.42 ± 0.27	Moderate

[a] Test concentration 5 μM; incubation time 2 h

[b] (P_{app} B to A) / (P_{app} A to B).

[c] Category criteria: low permeability, P_{app} A to B $\geq$ 3.0 and ER $\geq$ 10, or P_{app} A to B $<$ 3.0; moderate permeability, P_{app} A to B $\geq$ 3.0 and 10 $>$ ER $\geq$ 3; high permeability, P_{app} A to B $\geq$ 3.0 and 3.0 $>$ ER.

3. Conclusion

In conclusion, this study developed a novel series of acridine-containing hydroxamates by combining the core of HDAC and AChE inhibitor. Some of these compounds not only exhibited potent inhibiting activity against specific HDAC isoforms, but also significantly inhibited AChE. Two of these compounds, **6a** and **11b**, had excellent inhibitory activity against Aβ-aggregation and induced remarkable Aβ-oligomer disruption. These experimental findings suggest that the compounds were multi HDAC-Aβ-aggregation-AChE inhibitors. Compounds **6a** and **11b** significantly induced histone and tubulin acetylation. Notably, they can promote neurite outgrowth without significant neurotoxicity. These two compounds exhibited stability against microsome in the assay of microsome stability. Additionally, compound **11b** exhibited moderate BBB permeability. Further studies of the mechanisms of these multitarget inhibitors are ongoing.

4. Experimental

5.1. General procedures

NMR spectra (^{1}H and ^{13}C NMR) were obtained using the Bruker Fourier 300 and AVIII 500 spectrometer with standard plus programs. The chemical shifts were presented in parts per million (ppm, δ) with TMS as an internal standard. The MS data were measured on a Finnigan Mat TSQ-7000 mass spectrometer (ESIMS and HRESIMS). The melting point was recorded on a Fisher-Johns apparatus (uncorrected). HPLC was performed using a C18 column (150 mm × 4.6 mm, Ascentis) and an L-2130 pump (Hitachi, Ibaraki, Japan). Column chromatography was performed on silica gel (70-230 mesh, Merck, Darmstadt, Germany). The TLC analysis was performed on silica gel plates (KG60-F254, Merck). A microplate spectrophotometer Victor 2X (Perkin Elmer Fremont, CA, United States) was used for fluorometric analysis; an Envision 2104 Multilabel Reader (Perkin Elmer, CA, United States) was used for luminescence analysis, and a Sunrise microplate reader (TECAN, Männedorf, Switzerland) was used for absorbance analysis. Unless otherwise mentioned, all chemicals and materials were used as received from commercial suppliers without any purification. Anhydrous dichloromethane was distilled from calcium hydride under N_2.

*5.2. N-Hydroxy-4-(acridin-9-ylamino)benzamide (**6a**)*

To a solution of compound **4a** (72 mg, 0.47 mmol) and 9-chloroacridine **5** (100 mg, 0.47 mmol) in $CH_3O(CH_2)_2OH$ (1 mL) was added two drops of 12N $HCl_{(aq)}$. The resulting solution was stirred at RT and then concentrated in vacuo. The residue was diluted with distd H_2O (10 mL), neutralized with 1 N $HCl_{(aq)}$ to pH 7, and extracted with EtOAc (30 mL × 3). The organic layer was dried over Na_2SO_4 and filtered the solvent was then removed *in vacuo*. The residue was recrystallized from MeOH-THF (1: 9) to give **6a** (64 mg, 41%) as a solid. Mp 202-205 ^oC. IR (KBr) 3417, 3199, 1629, 1518, 1338, 1152 cm^{-1}. ^1H NMR (500 MHz, DMSO-d_6) δ 15.07(s, 1H), 11.62(s, 1H), 11.32(s, 1H), 8.29(d, *J* = 8.8 Hz, 2H), 8.16 (d, *J* = 8.8 Hz, 2H), 8.04 (t, *J* = 7.4 Hz, 2H), 7.86 (d, *J* = 8.8 Hz, 2H), 7.51 (d, *J* = 7.4 Hz, 2H), 7.48 (d, *J* = 8.8 Hz, 2H). ^{13}C NMR (125 MHz, DMSO-d_6) δ 163.3, 154.8, 140.2, 135.4, 133.4, 130.3, 128.4, 125.8, 124.1, 123.2, 119.4, 114.6. HRMS-ESI: m/z $[M+H]^+$ caclcd for $C_{20}H_{16}O_2N_3$ 330.1243, found 330.1237.

*5.3. N-Hydroxy-2-(4-(acridin-9-ylamino)phenyl)acetamide (**6b**)*

To a solution of reaction of **4b** (100 mg, 0.60 mmol) and 9-chloroacridine **5** (192 mg, 0.90 mmol) in $CH_3O(CH_2)_2OH$ (1 mL) was added two drops of 12N $HCl_{(aq)}$. Following the procedure as described for compound **6a**, the residue was recrystallized from EtOAc to give **6b** (107 mg, 52%) as a solid. Mp 209-210 ^oC. IR (KBr) 3443, 3124, 2990, 1670, 1514, 1273, 1167 cm^{-1}. ^1H NMR (300 MHz, CD_3OD) δ 8.20 (d, *J* =

8.8 Hz, 2H), 7.99 (m, 2H), 7.93 (m, 2H), 7.47 (t, *J* = 9.9 Hz, 2H), 7.41 (m, 4H), 3.52 (s, 2H). ^{13}C NMR (125 MHz, DMSO-d_6) δ 166.8, 155.2, 140.1, 139.4, 135.5, 135.4, 130.5, 125.7, 124.3, 123.8, 119.3, 113.7, 38.9. HRMS-ESI: m/z $[M+H]^+$ caclcd for $C_{21}H_{18}O_2N_3$ 344.1394, found 344.1384.

*5.4. N-Hydroxy-3-(4-(acridin-9-ylamino)phenyl)propanamide (**6c**)*

To a solution of **4c** (90 mg, 0.39 mmol), 9-chloroacridine **5** (125 mg, 0.59 mmol) in $CH_3O(CH_2)_2OH$ (1 mL) was added two drops of 12N $HCl_{(aq)}$. Following the procedure as described for compound **6a**, the residue was recrystallized from EtOAc to give **6c** (88 mg, 63%) as a solid. Mp 148-150 ^{o}C. IR (KBr) 3564, 3217, 3092, 1636, 1586, 1521, 1442, 1378, 1274 cm^{-1}. ^{1}H NMR (300 MHz, DMSO-d_6) δ 14.51 (s, 1H), 11.50 (s, 1H), 8.76 (s, 1H), 8.19 (d, *J* = 8.7 Hz, 2H), 8.00 (m, 4H), 7.42 (m, 2H), 7.34 (m, 4H), 3.04 (t, *J* = 7.4 Hz, 2H), 2.47 (t, *J* = 7.4 Hz, 2H). ^{13}C NMR (125 MHz, DMSO-d_6) δ 168.1, 155.3, 140.8, 140.1, 138.8, 135.4, 129.9, 125.8, 124.7, 123.8, 119.2, 113.5, 33.8, 30.5. HRMS-ESI: m/z $[M+H]^+$ caclcd for $C_{22}H_{20}O_2N_3$ 358.1550, found 358.1540.

*5.5. N-Hydroxy-3-(acridin-9-ylamino)benzamide (**6d**)*

To a solution of **4d** (72mg, 0.47mmol) and 9-chloroacridine **5** (100 mg, 0.47 mmol) in $CH_3O(CH_2)_2OH$ (1 mL) was added two drops of 12N $HCl_{(aq)}$. Following the procedure as described for compound **6a**, the residue was recrystallized from EtOAc

to give **6d** (88 mg, 57%) as a solid. Mp 224-225 ^{o}C. IR (KBr) 3382, 3164, 1636, 1579, 1558, 1520, 1474 cm^{-1}. ^{1}H NMR (500 MHz, CD_3OD) δ 8.20 (d, *J* = 8.8 Hz, 2H), 8.00 (m, 4H), 7.83 (s, 1H), 7.80 (d, *J* = 7.7 Hz, 1H), 7.61 (t, *J* = 8.0 Hz, 1H), 7.57 (d, *J* = 8.0 Hz, 1H), 7.47 (m, 2H). ^{13}C NMR (125 MHz, CD_3OD) δ 166.9, 155.4, 145.2, 143.0, 135.7, 135.4, 131.4, 128.8, 126.9, 125.3, 125.0, 122.6, 121.3, 116.9. HRMS-ESI: m/z $[M+H]^+$ caclcd for $C_{20}H_{16}O_2N_3$ 330.1237, found 330.1233.

*5.6. N-Hydroxy-4-(2-fluoroacridin-9-ylamino)benzamide (**11a**)*

To a solution of **10a** (100 mg, 0.43 mmol) and **4a** (63 mg, 0.41 mmol) in $CH_3O(CH_2)_2OH$ (1 mL) was added two drops of 12N $HCl_{(aq)}$. Following the procedure as described for compound **6a**, the residue was recrystallized from EtOAc to give **11a** (45 mg, 32%) as a solid. Mp 215-217 ^{o}C. IR (KBr) 3464, 3396, 1625, 1585, 1517, 1378 cm^{-1}. ^{1}H NMR (300 MHz, CD_3OD) δ 8.14 (d, *J* = 8.8 Hz, 1H), 8.08 (dd, *J* = 5.0, 9.4 Hz, 1H), 8.00 (m, 2H), 7.95 (t, *J* = 2.8 Hz, 1H), 7.93 (m, 1H), 7.89 (m, 2H), 7.50 (m, 1H), 7.44 (d, *J* = 8.6 Hz, 2H). ^{13}C NMR (125 MHz, DMSO-d_6) δ 163.3, 158.6, 156.7, 153.8, 140.5, 137.4, 135.2, 128.5, 125.7, 125.4, 124.2, 122.9, 122.7, 119.8, 119.6, 115.8, 114.3, 109.4, 109.2. HRMS -ESI m/z: $(M+H)^+$ caclcd for $C_{20}H_{15}O_2N_3F$ 348.1148, found 348.1143.

*5.7. N-Hydroxy-4-(2-bromoacridin-9-ylamino)benzamide (**11b**)*

To a solution of **10b** (100 mg, 0.34 mmol) and **4a** (56 mg, 0.37 mmol) in

$CH_3O(CH_2)_2OH$ (1 mL) was added two drops of 12N $HCl_{(aq)}$. Following the procedure as described for compound **6a**, the residue was recrystallized from EtOAc to give **11b** (58 mg, 41%) as a solid. Mp 264-267 ^oC. IR (KBr) 3233, 1557, 1500, 1416, 1264 cm^{-1}. ^1H NMR (300 MHz, CD_3OD) δ 8.48 (d, *J* = 2.0 Hz, 1H), 8.10 (m, 2H), 8.00 (m, 5H), 7.45 (m, 3H). ^{13}C NMR (125 MHz, DMSO-d_6) δ 164.2, 156.1, 151.5, 149.6, 139.2, 134.1, 131.9, 128.8, 128.1, 126.1, 125.4, 124.9, 117.7. HRMS-ESI: m/z $[M+H]^+$ caclcd for $C_{20}H_{15}O_2N_3Br$ 408.0348, found 408.0346.

*5.8. N-Hydroxy-4-(2-trifluoromethoxyacridin-9-ylamino)benzamide (**11c**)*

To a solution of **10c** (100 mg, 0.34mmol) and **4a** (55 mg, 0.36mmol) in $CH_3O(CH_2)_2OH$ (1 mL) was added two drops of 12N $HCl_{(aq)}$. Following the procedure as described for compound **6a**, the residue was recrystallized from EtOAc to give **11c** (65 mg, 46%) as a solid. Mp 130-134 ^oC. IR (KBr) 3381, 3164, 1641, 1586, 1514, 1273, 1253 cm^{-1}. ^1H-NMR (300 MHz, CD_3OD) δ 8.27 (d, *J* = 8.8 Hz, 1H), 8.08 (d, *J* = 9.4 Hz, 2H), 8.07 (m, 2H), 8.02 (m, 1H), 7.95 (m, 2H), 7.58 (m, 1H), 7.52 (d, *J* = 9.4 Hz, 2H). ^{13}C NMR (125 MHz, DMSO-d_6) δ 163.1, 155.0, 143.3, 140.4, 138.9, 135.8, 129.3, 128.6, 128.3, 125.7, 124.6, 123.6, 122.2, 121.0, 119.6, 119.0, 118.9, 117.2, 114.4. HRMS-ESI: m/z $[M+H]^+$ caclcd for $C_{21}H_{15}O_3N_3F_3$ 414.1066, found 414.1060.

*5.9. N-Hydroxy-4-(2-benzyloxyacridin-9-ylamino)benzamide (**11d**)*

To a solution **10d** (100 mg, 0.31 mmol) and **4a** (52 mg, 0.34 mmol) in $CH_3O(CH_2)_2OH$ (1 mL) was added two drops of 12N $HCl_{(aq)}$. Following the procedure as described for compound **6a**, the residue was recrystallized from EtOAc to give **11d** (42 mg, 31%) as a solid. Mp 123-125 ^oC. IR (KBr) 3381, 3148, 1632, 1583, 1508, 1498, 1419 cm^{-1}. ^1H NMR (300 MHz, CD_3OD) δ 8.26 (d, *J* = 8.8 Hz, 1H), 8.01 (m, 3H), 7.87 (d, *J* = 8.5 Hz, 2H), 7.80 (dd, *J* = 2.4, 9.4 Hz, 1H), 7.54 (m, 2H), 7.38 (d, *J* = 8.5 Hz, 2H), 7.32 (m, 5H), 4.94 (s, 2H). ^{13}C NMR (125 MHz, DMSO-d_6) δ 163.5, 154.9, 144.4, 139.6, 135.9, 134.5, 129.7, 128.9, 128.6, 128.4, 128.3, 127.9, 125.6, 122.7, 121.7, 119.9, 116.5, 114.9, 104.5, 70.2. HRMS-ESI: m/z $[M+H]^+$ caclcd for $C_{27}H_{22}O_3N_3$ 436.1661, found 436.1656.

*5.10. N-Hydroxy-4-(1,2,3-trimethoxyacridin-9-ylamino)benzamide (**11e**)*

To a solution of **10e** (100 mg, 0.33 mmol) and **4a** (53 mg, 0.34 mmol) in $CH_3O(CH_2)_2OH$ (1 mL) was added two drops of 12N $HCl_{(aq)}$. Following the procedure as described for compound **6a**, the residue was recrystallized from EtOAc to give **11e** (60 mg, 43%). Mp 210-213 ^oC. IR (KBr) 3418, 3234, 1634, 1585, 1489, 1422 cm^{-1}. ^1H NMR (500 MHz, DMSO-d_6) δ 14.77 (s, 1H), 11.25 (s, 1H), 9.03 (s, 1H), 8.02 (d, *J* = 8.5 Hz, 2H), 7.95 (d, *J* = 8.8 Hz, 2H), 7.92 (t, *J* = 7.7 Hz, 1H), 7.78 (d, *J* = 8.5 Hz, 2H), 7.35 (m, 4H), 4.07 (s, 3H), 3.94 (s, 3H), 3.81 (s, 3H). ^{13}C NMR (125 MHz, DMSO-d_6) δ 163.3, 160.2, 149.5, 144.2, 139.6, 139.4, 134.6, 129.7, 128.1,

125.8, 123.4, 121.8, 118.9, 113.9, 105.3, 94.4, 62.2, 61.3, 56.7. HRMS-ESI: m/z $[M+H]^+$ caclcd for $C_{23}H_{22}O_5N_3$ 420.1559, found 420.1559.

*5.11. N-Hydroxy-4-(7-chloro-2-methoxybenzo[b][1,5]naphthyridin-10-ylamino)benzamide (**11f**)*

To a solution of **10f** (100 mg, 0.36 mmol) and **4a** (58 mg, 0.38 mmol) in $CH_3O(CH_2)_2OH$ (1 mL) was added two drops of 12N $HCl_{(aq)}$. Following the procedure as described for compound **6a**, the residue was recrystallized from EtOAc to give **11f** (73 mg, 51%) as a solid. Mp 285-287 ^oC. IR (KBr) 3445, 1632, 1602, 1384, 1270 cm^{-1}. ^1H NMR (300 MHz, DMSO-d_6) δ 11.04 (s, 1H), 9.39 (s, 1H), 8.86 (s, 1H), 8.29 (d, *J* = 9.2 Hz,1H), 8.11 (d, *J* = 7.8 Hz, 2H), 7.66 (d, *J* = 8.6 Hz, 2H), 7.50 (dd, *J* = 2.2, 9.2 Hz, 1H), 7.34 (d, *J* = 8.6 Hz, 1H), 7.00 (d, *J* = 8.6 Hz, 2H), 3.69 (s, 3H). ^{13}C NMR (125 MHz, DMSO-d_6) δ 164.1, 159.5, 147.6, 147.0, 143.9, 141.4, 140.6, 134.0, 130.1, 129.8, 127.8, 127.5, 126.4, 125.1, 119.5, 118.8, 118.5, 117.8. HRMS-ESI: m/z $[M+H]^+$ caclcd for $C_{20}H_{16}O_3N_4Cl$ 395.0911, found 395.0905.

*5.12. N-Hydroxy-4-(5,6,7,8-tetrahydroacridin-9-ylamino)benzamide (**11g**)*

To a solution of **10g** (100 mg, 0.46 mmol) and **4a** (69 mg, 0.45 mmol) in $CH_3O(CH_2)_2OH$ (1 mL) was added two drops of 12N $HCl_{(aq)}$. Following the procedure as described for compound **6a**, the residue was recrystallized from EtOAc to give **11g** (40 mg, 0.12 mmol) as a solid. Mp 274-278 ^oC. IR (KBr) 3381, 3264,

2931, 1606, 1582, 1511, 1371, 1252 cm^{-1}. ^1H NMR (300 MHz, DMSO-d_6) δ 12.25 (s, 1H), 8.77 (s, 1H), 7.91 (d, *J* = 8.5 Hz,1H), 7.83 (dd, *J* = 0.8, 8.5 Hz,1H), 7.72 (d, *J* = 8.7 Hz, 2H), 7.64 (td, *J* = 1.4, 8.5 Hz, 1H), 7.43 (td, *J* = 1.4, 7.6 Hz, 1H), 6.58 (d, *J* = 8.7 Hz, 2H), 3.05 (t, *J* = 6.4 Hz, 2H), 2.69 (t, *J* = 6.4 Hz, 2H), 1.89 (m, 2H), 1.76 (m, 2H). ^{13}C NMR (125 MHz, DMSO-d_6) δ 167.7, 160.3, 150.1, 147.4, 142.2, 131.6, 129.1, 129.0, 126.5, 125.7, 124.3, 123.7, 120.4, 113.8, 33.9, 25.6, 22.8, 22.5. HRMS-ESI: m/z $[M+H]^+$ caclcd for $C_{20}H_{20}O_2N_3$ 334.1556, found 334.1550.

*5.13. N-Hydroxy-4-(quinolin-4-ylamino)benzamide (**11h**)*

To a solution of **10h** (100 mg, 0.61 mmol) and **4a** (82 mg, 0.54 mmol) in $CH_3O(CH_2)_2OH$ (1 mL) was added two drops of 12N $HCl_{(aq)}$. Following the procedure as described for compound **6a**, the residue was recrystallized from EtOAc to give **11h** (54 mg, 35%) as a solid. Mp 195-198 ^oC. IR (KBr) 3399, 3259, 2928, 1629, 1584, 1495, 1392, 1334 cm^{-1}. ^1H NMR (500 MHz, DMSO-d_6) δ 11.13 (s, 1H), 9.17 (s, 1H), 8.95 (s, 1H), 8.55 (d, *J* = 4.2 Hz,1H), 8.37 (d, *J* = 8.3 Hz, 1H), 7.91(d, *J* = 8.1 Hz, 1H), 7.79 (d, *J* = 8.4 Hz, 2H), 7.72(t, *J* = 7.3 Hz, 1H), 7.56 (t, *J* = 7.5 Hz, 1H), 7.41 (d, *J* = 8.0 Hz, 2H), 7.15 (d, *J* = 4.2 Hz, 1H). ^{13}C NMR (125 MHz, DMSO-d_6) δ 164.0, 150.7, 149.0, 146.5, 143.9, 129.5, 129.2, 128.3, 126.6, 125.0, 122.3, 120.4, 120.0, 103.5. HRMS-ESI: m/z [M+H]+ caclcd for $C_{16}H_{14}O_2N_3$ 280.1086, found 280.1080.

5.14. Preparation of HDAC4 and HDAC8

HDAC4 and HDAC8 was prepared as described previously[38]. Gene encoding HDAC4 (residue 648-1057) and HDAC8 (residue 1-377), flanked with Ndel and EcoR1 sites at the 5'- and 3'- ends, were synthesized by GenScript Corporation (NJ, USA) and subcloned into expression vectors pET-28a(+) and pET-24b(+), respectively. Proteins were expressed in BL21(DE3) cells by overnight induction with IPTG (1 mM) at 20-25 ^{o}C and purified from cleared cell lysates by sequential chromatography on Ni-Sepharose 6 fast flow, Mono Q 5/50 GL, and Superdex 75 10/300 GL columns (GE Healthcare). Protein concentrations were quantified using Bradford Reagent (Bio-Rad).

5.15. HDAC activity assay

The HDAC activity assay was performed as described previously [39]. Enzyme, inhibitors and substrate were diluted with HDAC buffer (15mM Tris-HCl pH 8.1, 0.25 mM EDTA, 250 mM NaCl, 10% v/v glycerol). Briefly, 10 μL diluted HDAC, i.e., HeLa nuclear extract (Enzo), HDAC1 (BPS), HDAC2 (BPS), HDAC3 (BPS), HDAC8, HDAC 4, HDAC 5 (BPS), HDAC6 (BPS), HDAC7 (BPS), HDAC9 (BPS) and 50 μL test compound solution at varying concentrations were added to each well of a 96-well microtiter plate and pre-incubated at 37 ºC for 5 min. The enzymatic reaction was started by the addition of 40 μL substrate, which was i.e.,

Boc-Lys(Ac)-AMC (BPS) for HeLa nuclear extract and HDAC6; Boc-Lys(TFA)-AMC (BPS) for HDAC4, -8; KI-177 (Enzo) for HDAC1, -2, -3; and 50040 (BPS) for HDAC5, -7, -9 in HDAC buffer. After incubation at 37 ºC for 30 min, the reaction was terminated by the addition of 100 µL trypsin solution (comprising 10 mg/mL trypsin in 50 mM Tris-HCl at pH 8, 100 mM NaCl, 2 mM SAHA). After incubation at 37 ºC for a further 20 min, fluorescence was measured (excitation λ= 355 nm, emission λ= 460 nm). To calculate IC_{50} values, the fluorescence in wells without the test compound (0.1% DMSO, negative control) was set as 100% enzymatic activity and the fluorescence in wells with 2 mM SAHA (positive control) was set at 0% enzymatic activity. All experiments were carried out in triplicate.

5.16. Inhibition of $A\beta_{1-42}$ aggregation

Inhibition of $A\beta_{1-42}$ self-aggregation measured by thioflavin-T (ThT) assay fluorescence assay was performed as described previously[40]. A 0.5 mg mass of $A\beta_{1-42}$ (Kelowna) was dissolved in 100 µL DMSO at RT to make a 1mM solution. Thioflavin-T stock with a concentration of 10 mM and inhibitors were diluted with 50 mM phosphate buffer (150 mM NaCl pH 7.4, 1 mM EDTA). Briefly, 25 µL test compound solution at varying concentrations and 100 µL working solution with or without $A\beta_{1-42}$ (10 µM ThT, 1 mM EDTA, and 10 µM $A\beta_{1-42}$ in 50 mM PB) were added to each well of a 96-well microtiter plate and incubated at 37 ºC and 700 rpm

on a BioShake iQ ThermoMixer for 24 h. After 24 h of incubation in 37ºC, $A\beta_{1-42}$ aggregation was assayed by significantly enhancing of ThT fluorescence in the presence of oligomerization. The fluorescence was measured (excitation λ= 440 nm, emission λ= 486 nm). To calculate IC_{50} values, the fluorescence in wells without the test compound (0.1% DMSO, negative control) was set as 100% $A\beta_{1-42}$ self-aggregation activity and the fluorescence in wells with various concentrations of compounds without $A\beta_{1-42}$ were set as background of various compounds as 0% $A\beta_{1-42}$ self-aggregation activity. All experiments were carried out in triplicate.

5.17. Disaggregation of aggregated $A\beta_{1-42}$

Disaggregation of aggregated $A\beta_{1-42}$ measured by thioflavin-T (ThT) assay fluorescence assay was performed as described in previous paragraph. Briefly, 100 μL working solution with or without $A\beta_{1-42}$ (10 μM ThT, 1 mM EDTA, and 10 μM $A\beta_{1-42}$ in 50 mM PB) was added to each well of a 96-well microtiter plate and incubated at 37 ºC and 700 rpm on a BioShake iQ ThermoMixer for 24 h. After 24 h incubation at 37 ºC, the fluorescence of the aggregated $A\beta_{1-42}$ was measured (excitation λ= 440 nm, emission λ= 486 nm). Then, 25 μL tested compound solution were added in the same 96-well microtiter plate and incubated at 37 ºC for another 24 h. After another 24 h incubation in 37ºC, the fluorescence was measured (excitation λ= 440 nm, emission λ= 486 nm). To calculate the $A\beta_{1-42}$ disaggregatory activity of each compound, the

value that was obtained by subtracting the second-measured fluorescence from the first-measured fluorescence was divided by the first-measured fluorescence. All experiments were carried out in triplicate.

5.18. AChE inhibition assay

The AChE inhibition assay was performed as described previously[41, 42]. AChE (Bio-Techne), inhibitors, acetylthiocholine iodide (ATCI) (Sigma-Aldrich), and 5,5-dithiobis(2-nitrobenzoic) acid (DTNB) (Sigma-Aldrich) were diluted with 100 mM phosphate buffer (pH 7.4). Briefly, 10 μL diluted AChE and 50 μL test compound solution at various concentrations were added to each well of a 96-well microtiter plate and pre-incubated at 37 ºC for 5 min. The enzymatic reaction was started by additing 20 μL acetylthiocholine iodide (1 mM) in phosphate buffer. After incubation at 37 ºC for 15 min, 20 μL DTNB (2 mM) was added to each well of a 96-well microtiter plate and incubated at 37 ºC for 5 min. The hydrolysis of acetylthiocholine was monitored at a wavelength of 412 nm. To calculate IC_{50} values, the absorbance in wells without the test compound (0.1% DMSO, negative control) was set as 100% enzymatic activity and the absorbance in wells without any enzyme were set at 0% enzymatic activity. All experiments were carried out in triplicate.

5.19. Cell viability CellTiter-Glo assay

Samples and the reference compound staurosporine were diluted in DMSO

solution with 10-dose and 2-fold dilutions (test compounds) or 3-fold dilutions (staurosporine) in a source plate, starting at a concentration of 10 mM. A 25 nL volume of each test compounds or staurosporine was delivered from the source plate to each well of 384-well cell culture plates using Echo 550. A 25 µL volume of culture medium that contained 1000 Neuro-2a cells was added to each of the wells of the cell culture plate. The cells were incubated with the compounds at 37 ºC in a humidified atmosphere of 5% CO_2 and 95% air for 24 hours. A 25 µL volume of Cell Titer Glo 2.0 reagent was added to each well. The contents were mixed on an orbital shaker for 2 min and incubated at room temperature for 15 min to stabilize the luminescence signal. Luminescence was recorded by an Envision 2104 Multilabel Reader (PerkinElmer, Santa Clara, CA). The number of viable cells in the culture was determined based on quantitation of the ATP present in each culture well. The IC_{50} curves were plotted and IC_{50} values were determined using a sigmoidal dose-response equation in the GraphPad Prism 4 program.

5.20. Western blot analysis

Neuro-2a cells were seeded at 0.3×10^6 cells/well in EMEM medium that contained 10% fetal bovine serum (FBS) for 24 h in a 12-well plate. The cells were treated with compounds, TSA or DMSO for 24 h. The final DMSO concentration in each culture sample was 0.2%. Compounds were tested in 10-dose IC_{50} mode with

2-fold serial dilution, starting at a concentration of 20 μM. The concentration of positive control compound TSA was 10 μM. After treatment, the culture medium was removed and the cells were washed once with ice-cold PBS. The cells were lysed with 1x Sample buffer that contained 50 mM DTT, and transferred to eppendorf tubes. The lysate samples were sheared and then heated at 90 ºC for 5 min. A 13 μL volume of cell lysate samples was separated by SDS-PAGE with 12% Tris-acetate gel and transferred onto nitrocellulose membranes using an iBlot dry blotting system (Life Technologies). The membranes were blocked with 2% non-fat milk for 1 h and probed with primary anti-Acetylated-histone H3K9 (C5B11) rabbit mAb (Cell Signaling Technology), anti-histone H3 (96C10) mouse mAb (Cell Signaling Technology), anti-Acetylated-α-tubulin mouse mAb (Sigma-Aldrich), and anti-α-tubulin rabbit Ab, respectively. Anti-rabbit IgG IRDye 680RD (LI-COR) and anti-mouse IgG IRDye 800CW secondary antibodies (LI-COR) were used to detect the primary antibodies. The membranes were scanned using an LI-COR Odyssey Fc Imaging System. The specific signals of the bands of interest were quantified using the LI-COR Odyssey Fc Imaging System. The EC_{50} values of the testing compounds were calculated using a sigmoidal dose-response equation in the GraphPad Prism 4 program.

5.21. Neurite outgrowth assay

Primary hippocampus tissue from pregnant Sparague-Dawley rat embryos was digested and centrifuged in a plating medium (minimal essential medium, containing 5% FBS (Invitrogen) and 5% HS (HyClone)). The cell pellet thus obtained was cultured into poly-D-lysine-coated wells of a 12-well plate or a 24-well plate in 37□ in a humidified atmosphere of 5% CO_2 and 95% air for 24 hours. The plating medium was replaced with neurobasal medium (2% B27-neurobasal medium (Invitrogen), containing 0.5 mM glutamine, and 12.5 μM glutamic acid). Primary hippocampus neurons from SD rat embryos were treated with DMSO or compounds for three days from the third day *in vitro* (DIV3) and fixed at DIV6 with 4% paraformaldehyde in PBS. Neurites were stained with primary anti-tau mouse Ab (Invitrogen) and anti-MAP2 rabbit Ab (Millipore); nuclei were visualized after staining with DAPI. Donkey anti-mouse IgG conjugated Alexa Flour ®488 and Donkey anti-rabbit IgG conjugated Alexa Flour ®594 secondary antibodies (Abcam) were used to detect the primary antibodies. Images were recorded using Zeiss Axio observer. D1 fluorescence microscopes. At least 20 neuronal cells were chosen, recorded, analyzed, and quantified for their number, length, and total output (sum of length) of primary, secondary, and tertiary neurites of axons and dendrites using the semi-automated tracing program ImageJ.

5.22. Microsome stability assay

Mixed-gender human liver microsomes (Lot# 1710084) were purchased from XenoTech. The reaction mixture minus NADPH was prepared as described below. The test article was added to the reaction mixture at a final concentration of 1 µM. The control compound, testosterone (5 µM), was run simultaneously with the test articles in a separate reaction. An aliquot of the reaction mixture (without cofactor) was equilibrated in a shaking water bath at 37°C for 3 minutes. The reaction was initiated by adding a cofactor, and the mixture was incubated in a shaking water bath at 37°C. Aliquots (100 µL) were withdrawn at 0, 10, 20, 30, and 60 minutes from the wells of the test articles and testosterone. Test article and testosterone samples were immediately combined with 400 µL of ice-cold 50/50 acetonitrile (ACN)/H_2O, containing 0.1% formic acid and an internal standard to terminate the reaction. The samples were then mixed and centrifuged to precipitate proteins. All samples were assayed by LC-MS/MS using electrospray ionization. The peak area response ratio (PARR) to internal standard was compared to the PARR at time 0 to determine the percentage of test articles remaining at each time point. Half-lives were calculated by Absorption Systems LLC (Exton, PA) using GraphPad software, with fitting to a single-phase exponential decay equation.

5.23. MDR1-MDCK permeability assay

MDR1-MDCK cell monolayers were grown to confluence on collagen-coated,

microporous membranes in 12-well assay plates. Details of the plates and their certification are shown below. The permeability assay buffer was Hanks' balanced salt solution, which contained 10 mM HEPES and 15 mM glucose at a pH of 7.4. The buffer in the receiver chamber also contained 1% bovine serum albumin. The dosing solution concentration was 5 µM of the test article in the assay buffer. Cell monolayers were dosed on the apical side (A-to-B) or basolateral side (B-to-A) and incubated at 37°C with 5% CO_2 in a humidified incubator. Samples were taken from the donor and receiver chambers at 120 minutes. Each determination was performed in duplicate. The flux of lucifer yellow was also measured post-experimentally on each monolayers to ensure that no damage was done to the cell monolayers during the flux period. All samples were assayed by LC-MS/MS using electrospray ionization. The apparent permeability (P_{app}) and percentage recovery were calculated by Absorption Systems LLC (Exton, PA) as follows.

$$\mathrm{P_{app}} = (d\mathrm{C_r}/d\mathrm{t}) \times \mathrm{V_r}(\mathrm{A} \times \mathrm{C_A})$$

$$\text{Percent Recovery } = 100 \times \left(\left(\mathrm{V_r} \times \mathrm{C_r}^{\mathrm{final}}\right) + \left(\mathrm{V_d} \times \mathrm{C_d}^{\mathrm{final}}\right)\right)/(\mathrm{V_d} \times \mathrm{C_N})$$

$$\text{Efflux ratio (ER) is defined as } \mathrm{P_{app}}(\mathrm{B-to-A})/\mathrm{P_{app}}(\mathrm{A-to-B})$$

Acknowledgements. We gratefully acknowledge the support from the Ministry of Science and Technology (MOST108-2320-B-038 -036 and MOST108-2320-B-038-058-MY3) in Taiwan. This research was also partially

supported by the Taiwan Protein Project (Grant No. MOST105-0210-01-12-01 and Grant No. MOST106-0210-01-15-04).

References

[1] R. Leon, A.G. Garcia, J. Marco-Contelles, Recent advances in the multitarget-directed ligands approach for the treatment of Alzheimer's disease, Med. Res. Rev. 33 (2013) 139-189.

[2] G.R. Zimmermann, J. Lehar, C.T. Keith, Multi-target therapeutics: when the whole is greater than the sum of the parts, Drug Discov. Today 12 (2007) 34-42.

[3] J.L. Medina-Franco, M.A. Giulianotti, G.S. Welmaker, R.A. Houghten, Shifting from the single to the multitarget paradigm in drug discovery, Drug Discov. Today 18 (2013) 495-501.

[4] R.R. Ramsay, M.R. Popovic-Nikolic, K. Nikolic, E. Uliassi, M.L. Bolognesi, A perspective on multi-target drug discovery and design for complex diseases, Clin. Transl. Med. 7 (2018) 3.

[5] N. Guzior, A. Wieckowska, D. Panek, B. Malawska, Recent development of multifunctional agents as potential drug candidates for the treatment of Alzheimer's disease, Curr. Med. Chem. 22 (2015) 373-404.

[6] C.J. Van der Schyf, The use of multi-target drugs in the treatment of neurodegenerative diseases, Expert Rev. Clin. Pharmacol. 4 (2011) 293-298.

[7] C. Hubbert, A. Guardiola, R. Shao, Y. Kawaguchi, A. Ito, A. Nixon, M. Yoshida, X.F. Wang, T.P. Yao, HDAC6 is a microtubule-associated deacetylase, Nature 417 (2002) 455-458.

[8] B.J. North, B.L. Marshall, M.T. Borra, J.M. Denu, E. Verdin, The human Sir2 ortholog, SIRT2, is an NAD+-dependent tubulin deacetylase, Mol. Cell 11 (2003) 437-444.

[9] L. Mahady, M. Nadeem, M. Malek-Ahmadi, K.W. Chen, S.E. Perez, E.J. Mufson, Frontal Cortex Epigenetic Dysregulation During the Progression of Alzheimer's Disease, J. Alzheimers Dis. 62 (2018) 115-131.

[10] J. Graff, D. Rei, J.S. Guan, W.Y. Wang, J. Seo, K.M. Hennig, T.J.F. Nieland, D.M. Fass, P.F. Kao, M. Kahn, S.C. Su, A. Samiei, N. Joseph, S.J. Haggarty, I. Delalle, L.H. Tsai, An epigenetic blockade of cognitive functions in the neurodegenerating brain, Nature 483 (2012) 222-226.

[11] H. Yamakawa, J. Cheng, J. Penney, F. Gao, R. Rueda, J. Wang, S. Yamakawa, O. Kritskiy, E. Gjoneska, L.H. Tsai, The Transcription Factor Sp3 Cooperates with HDAC2 to Regulate Synaptic Function and Plasticity in Neurons, Cell Rep. 20 (2017) 1319-1334.

[12] J.L. Li, J.M. Chen, C.L. Ricupero, R.P. Hart, M.S. Schwartz, A. Kusnecov, K. Herrup, Nuclear accumulation of HDAC4 in ATM deficiency promotes neurodegeneration in ataxia telangiectasia, Nat. Med. 18 (2012) 783-790.

[13] N. Govindarajan, P. Rao, S. Burkhardt, F. Sananbenesi, O.M. Schluter, F. Bradke, J. Lu, A. Fischer, Reducing HDAC6 ameliorates cognitive deficits in a mouse model for Alzheimer's disease, EMBO Mol. Med. 5 (2013) 52-63.

[14] C. Ballatore, K.R. Brunden, J.Q. Trojanowski, V.M.Y. Lee, A.B. Smith, D.M. Huryn, Modulation of Protein-Protein Interactions as a Therapeutic Strategy for the treatment of neurodegenerative tauopathies, Curr. Top. Med. Chem. 11 (2011) 317-330.

[15] J.H. Tseng, L. Xie, S. Song, Y.M. Xie, L. Allen, D. Ajit, J.S. Hong, X. Chen, R.B. Meeker, T.J. Cohen, The deacetylase HDAC6 mediates endogenous neuritic tau pathology, Cell Rep. 20 (2017) 2169-2183.

[16] C.W. Yu, P.T. Chang, L.W. Hsin, J.W. Chern, Quinazolin-4-one derivatives as selective histone deacetylase-6 inhibitors for the treatment of Alzheimer's disease, J. Med. Chem. 56 (2013) 6775-6791.

[17] D.M. Chuang, Y. Leng, Z. Marinova, H.J. Kim, C.T. Chiu, Multiple roles of HDAC inhibition in neurodegenerative conditions, Trends Neurosci. 32 (2009) 591-601.

[18] S.S. Yang, R. Zhang, G. Wang, Y.F. Zhang, The development prospection of HDAC inhibitors as a potential therapeutic direction in Alzheimer's disease, Transl. Neurodegener. 6 (2017) 19.

[19] E. Viayna, T. Gomez, C. Galdeano, L. Ramirez, M. Ratia, A. Badia, M.V. Clos, E. Verdaguer, F. Junyent, A. Camins, M. Pallas, M. Bartolini, F. Mancini, V. Andrisano, M.P. Arce, M.I. Rodriguez-Franco, A. Bidon-Chanal, F.J. Luque, P. Camps, D. Munoz-Torrero, Novel huprine derivatives with inhibitory activity toward beta-amyloid aggregation and formation as disease-modifying anti-Alzheimer drug candidates, ChemMedChem 5 (2010) 1855-1870.

[20] M.Y. Wu, G. Esteban, S. Brogi, M. Shionoya, L. Wang, G. Campiani, M. Unzeta, T. Inokuchi, S. Butini, J. Marco-Contelles, Donepezil-like multifunctional agents: Design, synthesis, molecular modeling and biological evaluation, Eur. J. Med. Chem. 121 (2016) 864-879.

[21] O. Bar-Am, O. Weinreb, T. Amit, M.B.H. Youdim, The novel cholinesterase-monoamine oxidase inhibitor and antioxidant, ladostigil, confers neuroprotection in neuroblastoma cells and aged rats, J. Mol. Neurosci. 37 (2009) 135-145.

[22] J. Marco-Contelles, R. Leon, C. de los Rios, A. Samadi, M. Bartolini, V. Andrisano, O. Huertas, X. Barril, F.J. Luque, M.I. Rodriguez-Franco, B. Lopez, M.G. Lopez, A.G. Garcia, M. do Carmo Carreiras, M. Villarroya, Tacripyrines, the first tacrine-dihydropyridine hybrids, as multitarget-directed ligands for the treatment of Alzheimer's disease, J. Med. Chem. 52 (2009) 2724-2732.

[23] G.F. Makhaeva, S.V. Lushchekina, N.P. Boltneva, O.G. Serebryakova, E.V. Rudakova, A.A. Ustyugov, S.O. Bachurin, A.V. Shchepochkin, O.N. Chupakhin, V.N. Charushin, R.J. Richardson, 9-Substituted acridine derivatives as acetylcholinesterase and butyrylcholinesterase inhibitors possessing antioxidant activity for Alzheimer's disease treatment, Bioorg. Med. Chem. 25 (2017) 5981-5994.

[24] S. Hamulakova, J. Imrich, L. Janovec, P. Kristian, I. Danihel, O. Holas, M. Pohanka, S. Bohm, M. Kozurkova, K. Kuca, Novel tacrine/acridine anticholinesterase inhibitors with piperazine and thiourea linkers, Int. J. Biol. Macromol. 70 (2014) 435-439.

[25] T. Fuchigami, N. Kobashi, M. Haratake, M. Kawasaki, M. Nakayama, Synthesis and biological evaluation of radioiodinated quinacrine-based derivatives for SPECT imaging of Abeta plaques, Eur. J Med. Chem. 60 (2013) 469-478.

[26] A. Antosova, B. Chelli, E. Bystrenova, K. Siposova, F. Valle, J. Imrich, M. Vilkova, P. Kristian, F. Biscarini, Z. Gazova, Structure-activity relationship of acridine derivatives to amyloid aggregation of lysozyme, Biochim. Biophys. Acta 1810 (2011) 465-474.

[27] X.Y. Jiang, T.K. Chen, J.T. Zhou, S.Y. He, H.Y. Yang, Y. Chen, W. Qu, F. Feng, H.P. Sun, Dual GSK-3beta/AChE inhibitors as a new strategy for multitargeting anti-Alzheimer's disease drug discovery, ACS Med. Chem. Lett. 9 (2018) 171-176.

[28] L. Ismaili, M. do Carmo Carreiras, Multicomponent reactions for multitargeted compounds for Alzheimer`s disease, Curr. Top. Med. Chem. 17 (2017) 3319-3327.

[29] A. Romero, R. Cacabelos, M.J. Oset-Gasque, A. Samadi, J. Marco-Contelles, Novel tacrine-related drugs as potential candidates for the treatment of Alzheimer's disease, Bioorg. Med. Chem. Lett. 23 (2013) 1916-1922.

[30] S. Carta, S. Tassi, C. Semino, G. Fossati, P. Mascagni, C.A. Dinarello, A. Rubartelli, Histone deacetylase inhibitors prevent exocytosis of interleukin-1beta-containing secretory lysosomes: role of microtubules, Blood 108 (2006) 1618-1626.

[31] J.J. Buggy, Z.A. Cao, K.E. Bass, E. Verner, S. Balasubramanian, L. Liu, B.E. Schultz, P.R. Young, S.A. Dalrymple, CRA-024781: a novel synthetic inhibitor of histone deacetylase enzymes with antitumor activity in vitro and in vivo, Mol. Cancer Ther. 5 (2006) 1309-1317.

[32] J.H. Kalin, K.V. Butler, T. Akimova, W.W. Hancock, A.P. Kozikowski, Second-generation histone deacetylase 6 inhibitors enhance the immunosuppressive effects of Foxp3+ T-regulatory cells, J. Med. Chem. 55 (2012) 639-651.

[33] T. Suzuki, Y. Ota, M. Ri, M. Bando, A. Gotoh, Y. Itoh, H. Tsumoto, P.R. Tatum, T. Mizukami, H. Nakagawa, S. Iida, R. Ueda, K. Shirahige, N. Miyata, Rapid discovery of highly potent and selective inhibitors of histone deacetylase 8 using click chemistry

to generate candidate libraries, J. Med. Chem. 55 (2012) 9562-9575.
[34] J.B. Houston, Utility of in vitro drug metabolism data in predicting in vivo metabolic clearance, Biochem. Pharmacol. 47 (1994) 1469-1479.
[35] X.N. Jin, T.L. Luong, N. Reese, H. Gaona, V. Collazo-Velez, C. Vuong, B. Potter, J.C. Sousa, R. Olmeda, Q.G. Li, L.S. Xie, J. Zhang, P. Zhang, G. Reichard, V. Melendez, S.R. Marcsisin, B.S. Pybus, Comparison of MDCK-MDR1 and Caco-2 cell based permeability assays for anti-malarial drug screening and drug investigations, J. Pharmacol. Toxicol. Methods 70 (2014) 188-194.
[36] K.M.M. Doan, J.E. Humphreys, L.O. Webster, S.A. Wring, L.J. Shampine, C.J. Serabjit-Singh, K.K. Adkison, J.W. Polli, Passive permeability and P-glycoprotein-mediated efflux differentiate central nervous system (CNS) and non-CNS marketed drugs, J. Pharmacol. Exp. Ther. 303 (2002) 1029-1037.
[37] Q. Wang, J.D. Rager, K. Weinstein, P.S. Kardos, G.L. Dobson, J.B. Li, I.J. Hidalgo, Evaluation of the MDR-MDCK cell line as a permeability screen for the blood-brain barrier, Int. J. Pharm. 288 (2005) 349-359.
[38] S.W. Chao, L.C. Chen, C.C. Yu, C.Y. Liu, T.E. Lin, J.H. Guh, C.Y. Wang, C.Y. Chen, K.C. Hsu, W.J. Huang, Discovery of aliphatic-chain hydroxamates containing indole derivatives with potent class I histone deacetylase inhibitory activities, Eur. J. Med. Chem. 143 (2018) 792-805.
[39] W.J. Huang, Y.C. Wang, S.W. Chao, C.Y. Yang, L.C. Chen, M.H. Lin, W.C. Hou, M.Y. Chen, T.L. Lee, P. Yang, C.I. Chang, Synthesis and biological evaluation of ortho-aryl N-hydroxycinnamides as potent histone deacetylase (HDAC) 8 isoform-selective inhibitors, ChemMedChem 7 (2012) 1815-1824.
[40] L.C. Chen, H.J. Tseng, C.Y. Liu, Y.Y. Huang, C.C. Yen, J.R. Weng, Y.L. Lu, W.C. Hou, T.E. Lin, I.H. Pan, K.K. Huang, W.J. Huang, K.C. Hsu, Design of diarylheptanoid derivatives as dual inhibitors against class IIa histone deacetylase and beta-amyloid aggregation, Front. Pharmacol. 9 (2018) 708.
[41] L. Peauger, R. Azzouz, V. Gembus, M.L. Tintas, J.S.D. Santos, P. Bohn, C. Papamicael, V. Levacher, Donepezil-based central acetylcholinesterase inhibitors by means of a "bio-oxidizable" prodrug strategy: design, synthesis, and in vitro biological evaluation, J. Med. Chem. 60 (2017) 5909-5926.
[42] G.L. Ellman, K.D. Courtney, V. Andres, Jr., R.M. Feather-Stone, A new and rapid colorimetric determination of acetylcholinesterase activity, Biochem Pharmacol. 7 (1961) 88-95.

1. Novel acridine-containing histone deacetylase inhibitors have been developed.
2. Structure-activity relationship of the resulting compounds has been established.
3. Several compounds are identified as multiple HDAC-Aβ-aggregation-AChE inhibitors.
4. Compounds **11b** and **6a** enhance neurite outgrowth without significant neurotoxicity.
5. Compound **11b** can permeate blood-brain barrier.

Declaration of interests

☒ The authors declare that they have no known competing financial interests or personal relationships that could have appeared to influence the work reported in this paper.

☐The authors declare the following financial interests/personal relationships which may be considered as potential competing interests: